

Short-Delay Multipath Errors in NavIC Signals for Stationary Receivers^{*}

Kartik Tiwari¹, Althaf A², and Hari Hablani³

¹ Ashoka University, Delhi-NCR, India kartik.tiwari_ug22@ashoka.edu.in

² Indian Institute of Technology, Indore, India phd1601121012@iiti.ac.in

³ Indian Institute of Technology, Indore, India hhablani@iiti.ac.in

Abstract. This paper presents, in part, a tutorial overview of the code phase error and carrier phase error caused by a single reflected path and an iterative algorithm to determine the root of the well-known multipath-affected discriminator function. The algorithm is then applied to determine the code error and carrier phase error in GPS signals in a single reflected path environment, and is validated by comparing the results with the known results. The algorithm is further used to determine and illustrate single-path errors in NavIC (Navigation with Indian Constellation) signals for the first time in the literature. The NavIC errors differ significantly from the GPS errors because of the limited and slow traverses of the elevation and azimuth angles of the three geostationary and four geosynchronous NavIC satellites signals to a stationary receiver on the ground. NavIC multipath errors of a real receiver on the ground for both L5 and S1 frequencies are presented. The multipath errors of the two frequencies differ greatly because the S1 wavelength (0.12 m) is nearly half of the L5 wavelength (0.25 m) and, therefore, the S1 multipath error frequencies are nearly twice of the L5 multipath error frequencies. The real multipath errors differ from the ideal single-path ground reflection errors because, in reality, the diffractors may be multiple comprising both horizontal and vertical, and the reflections vary with time due to both elevation and azimuth of the satellite signals, causing substantial disorder in errors.

Keywords: NavIC · Multipath · Navigation · Signal

1 Introduction

It is possible for receivers to receive direct navigation signals from satellites affected by delayed, reflected signals. Such reflections can be caused by objects surrounding the receivers like high-rise buildings, satellite dishes on the terraces in urban settings, or ground diffractors. Multipath error can lead to loss of accuracy in the position, velocity and time estimates using the navigation satellites

^{*} This research was supported by Space Applications Center, Indian Space Research Organization as a part of NGP-17 project. *Manuscript presented at the 72nd International Astronautical Congress, Dubai, 2021-10-28. Copyright by IAF*

such as NavIC (Navigation with Indian Constellation). Multipath errors are well understood for the GPS signals. This document discusses our attempts to identify and understand multipath error for NavIC frequencies.

The paper is organized as follows. Secs.II-VI provide a tutorial on short-delay multipath errors. Sec. II illustrates the ideal, triangle autocorrelation function – a central element of the delay lock loop. Sec. III presents the formulation and illustration of maximum phase error and fading and enhancement of the direct signal caused by a single reflected signal. Sec. IV outlines the early and late correlators and illustrates the ideal discriminator functions for wide and narrow correlators. Sec. V illustrates the distortion of the triangle autocorrelation function by a single reflected signal, which causes errors in determination of the root of the discriminator function. The nonlinear, coupled equations of the code phase errors and carrier phase errors caused by a single-path reflection and an iterative algorithm to solve them are presented in Sec. VI. The algorithm is applied to GPS signals in Sec. VII and results are compared with the known code phase and carrier phase errors for validation of the software. The validated algorithm is applied to the NavIC signals of L5 and S1 frequency bands. Sec. VIII summarizes the equations of code phase multipath error envelopes and non-zero mean errors, and illustrates them for NavIC signals. Sec. IX presents a case study of real multipath errors in the NavIC signals using an Accord receiver and an antenna. Relationships of the additional reflected path length with elevation and azimuth angles of the signal, and thus time, are summarized. Frequency bandwidth of the reflected signal and its influence on the accuracy specifications of Doppler shift is explored. Real multipath errors of NavIC signals and their relationship with the elevation and azimuth angles of the satellites are presented. Sec. X concludes the paper.

2 Code Auto-Correlation - No Multipath Error

The receiver maintains an exact replica of the code that it receives from a particular navigation satellite signal and measures the relative time delay between the satellite code and the receiver replica. This delay is then used to calculate the receiver distance to that satellite. Once the distances to at least four such navigation satellites are known, the receiver proceeds to solve a set of four equations that yield the position of the receiver and its clock bias with the NavIC or GNSS system time reference. A principal element of this measurement process is the determination of correlation between the received signal and the receiver-generated signal, implemented in a delay lock loop (DLL) in the receiver.

2.1 Satellite Pseudorandom Code

The satellite code is a pseudo-random code of 1023 (equivalently, $2^{10} - 1$) chips repeating every millisecond. This implies that each chip pulse width is $(1/1023)\text{ms} = 0.9775\mu\text{s} \approx 1\mu\text{s}$. The satellite code is multiplied with receiver's replica of the code and averaged as explained in [2]. At zero time delay estimation error ($\Delta\tau = 0$),

the normalized value of the correlation is equal to 1. This value of 1, or the peak, is what the autocorrelation algorithm seeks.

EXAMPLE 1: Auto correlation Code [1]

Suppose the carrier code is (+1, -1, -1, +1, -1) and the receiver's replica being correlated is (+1, -1, +1, -1, -1). The product of each term then becomes (+1, +1, -1, -1, +1). Taking the sum of all bits and dividing the sum by 5 gives us the value 0.2 instead of 1 which we would get if the two codes were the same. Therefore, the receiver replica code is not for this satellite and the receiver will look for a signal for which the correlation is 1.

2.2 Delay Lock Loop

As mentioned previously, at zero delay estimation error ($\Delta\tau = 0$), the normalized auto-correlation value becomes 1. For an uncorrupted signal, this is the highest possible value of the output of an auto-correlation function. A receiver, thus, tries to find this auto-correlation peak in order to measure the time delay. Delay Lock Loops are used for this process. *Misra and Enge* [2] in Chapter 10 describe a basic DLL as the following:

... the delay lock loop correlates the received Signal with a slightly early replica of the Signal and a slightly late replica of the signal. When locked to the received Signal, the early correlator samples the peak of the correlation function on the rising edge, and the late correlator samples the peak on the falling edge.

In the delay lock loop, a navigation signal affected by its reflected signal does not produce the expected ideal correlation triangle between a direct satellite signal and the receiver-generated pure pseudo-random code. The ideal correlation triangle is shown in Fig. 1 while perturbed correlation triangles will be shown in Sec. V.

Because of perturbation in the correlation triangle, the discriminator function – the early correlator triangle minus the late correlator triangle – is distorted and its root does not yield the correct value of the signal arrival delay. The delay estimation error, in nanoseconds, thus caused by the reflected signal is the multipath error, and it is illustrated in Sec. VI (also see [8]).

The algorithm and the software we developed is first validated by comparing our multipath error results for GPS with the results in the literature. The software then is used to generate the multipath error results for the NavIC signals.

2.3 Autocorrelation Function

Autocorrelation is a function of the unknown signal time delay τ . Denoting its estimate as τ^* , the residual estimation error is denoted $\Delta\tau$. So, the autocorre-

lation as a function of $\Delta\tau$ is [Chapter 9, 2]

$$R(\Delta\tau) = \begin{cases} \frac{\Delta\tau}{T_C} + 1 & \text{if } -T_C < \Delta\tau < 0 \\ 1 - \frac{\Delta\tau}{T_C} & \text{if } 0 < \Delta\tau < T_C \\ 0 & \text{otherwise} \end{cases} \quad (1)$$

where T_C (chip pulse width) is equal to $0.9775 \mu\text{s}$. As demonstrated in Fig 1, the autocorrelation function has a sharp and distinct peak when $\Delta\tau = 0$.

Since this paper deals exclusively with the multipath error, $\Delta\tau$ in this paper represents the delay of the multipath relative to the direct signal, denoted $\Delta\tau_M$ in *Misra-Enge* [2].

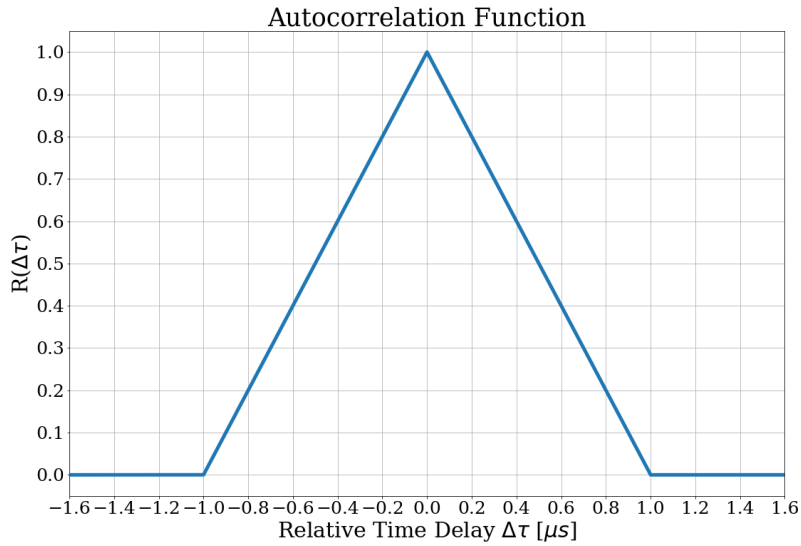


Fig. 1. Uncorrupted Autocorrelation Peak with its peak at $\Delta\tau = 0$

3 Phase and Amplitude Errors Caused by Single Reflected Signal

Suppose $\Delta\tau_M$ denotes the extra time a reflected signal takes to reach the receiver antenna relative to the direct signal from a satellite. The reflecting surface may be the ground supporting the antenna or may be a wall in the neighborhood, reflecting the navigation signal, and the reflected signal traverses an extra distance Δl relative to the direct signal. Clearly, $\Delta l = c\Delta\tau_M$, where c is the speed

of light. Δl would depend on the direct signal elevation and azimuth angle of the reflector relative to the signal. See more about it in Sec. VIII.

Doherty et al. [3] analyzed signal strength variation in the presence of reflected signals, determined the maximum perturbation in the phase of the signal before entering the receiver software and the code phase error caused by the reflected signal. Because of their fundamental importance, signal strength variation and phase perturbations are summarized below. Denote (see Fig. 2).

V_D = Directly received signal voltage

V_R = Reflected signal voltage

R = Resultant voltage

θ_m = Phase difference between directly received and reflected signal.

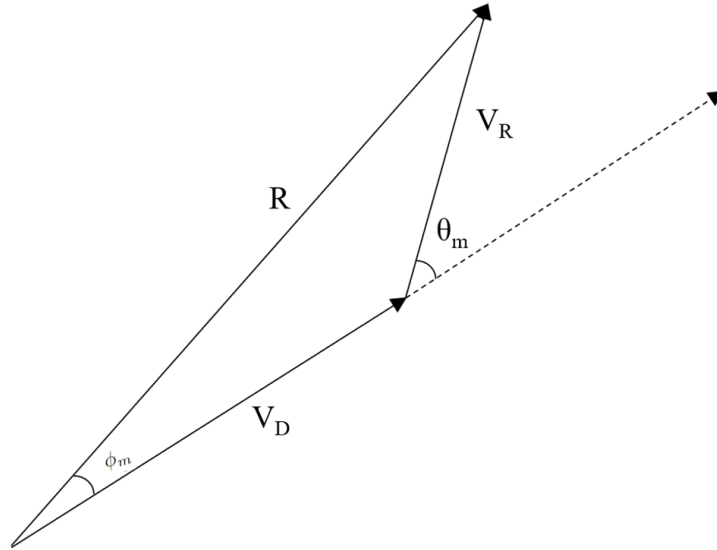


Fig. 2. An illustration of the vectorial addition of reflected signal and direct signal to form the resultant composite signal

As mentioned earlier, the resultant signal is a vector sum of the direct signal and reflected signal. This is illustrated in the Fig. 2. From Fig. 2, *Hofman-Wellenhof et al.* [10] show that the change in the phase angle of the direct carrier signal due to the reflected signal is

$$\tan \phi_m = \frac{(V_R/V_D) \sin \theta_m}{1 + (V_R/V_D) \cos \theta_m} \quad (2)$$

The zero-slope condition of $\tan \phi_m$ with respect to θ_m gives the following θ_m^* for maximum $\tan \phi_m$

$$\frac{d}{d\theta_m} \left[\frac{\sin \theta_m}{1 + (V_R/V_D) \cos \theta_m} \right] = 0 \quad (3)$$

$$\implies \theta_m^* = \cos^{-1} \left(-\frac{V_R}{V_D} \right)$$

Substituting $\cos \theta_m^*$ and the corresponding $\sin \theta_m^*$, the maximum perturbation in the carrier phase, denoted $\phi_{m_{max}}$, caused by the reflected signal reaching the antenna is found to be

$$\tan \phi_{m_{max}} = \frac{(V_R/V_D)}{\sqrt{1 - (V_R/V_D)^2}} \quad (4)$$

which, more simply, is

$$\phi_{m_{max}} = \sin^{-1} (V_R/V_D) \quad (5)$$

Direct signal is enhanced, or constructively interfered, when the reflected signal is in sync (in phase, θ_m in Fig. 2 equals zero) with the direct signal. The maximally enhanced signal, then, normalized with its direct value is, in dB,

$$\begin{aligned} E_m &= 20 \log_{10}(V_D + V_R)/V_D \\ &= 20 \log_{10}(1 + \sin \phi_{m_{max}}) \end{aligned}$$

(E for enhanced). Similarly, when the reflected signal and the direct signal are out of phase (θ_m in Fig. 2 equals 180°), the direct signal is destructively interfered and it experiences a fade. The maximally faded signal, normalized with V_D , is then, in dB

$$\begin{aligned} F_m &= 20 \log_{10}(V_D - V_R)/V_D \\ &= 20 \log_{10}(1 - \sin \phi_{m_{max}}) \end{aligned}$$

(F for faded). The total variation in signal is the sum of max fade and max enhancement. These relations are demonstrated in Fig. 3, following [3]. As in [3], Fig. 3 is used by picking a value of V_D/V_R in decibels from the x-axis and finding its corresponding value of $\phi_{m_{max}}$ on the y-axis. From there, look for the corresponding values of max fade, max enhancement and total variation in the signal strength, all on the x-axis for the $\phi_{m_{max}}$ specified.

EXAMPLE 2: $V_D/V_R = 20\text{dB}$

This is an extreme example of nearly no reflection since $V_D/V_R = 10^{20/20} = 10$,

$$V_R/V_D = 0.1 = \sin(\phi_{m_{max}}) \implies \phi_{m_{max}} = 5.74^\circ$$

The Max Fade F_m becomes

$$\begin{aligned} F_m &= 20 \log_{10}(1 - \sin \phi_{m_{max}}) = 20 \log_{10}(1 - 0.1) \\ F_m &= 20 \log_{10}(0.9) = -0.92\text{dB} \end{aligned}$$

The Max Enhancement E_m is

$$\begin{aligned} E_m &= 20 \log_{10}(1 + \sin \phi_{m_{max}}) = 20 \log_{10}(1 + 0.1) \\ E_m &= 20 \log_{10}(1.1) = 0.83\text{dB} \end{aligned}$$

E_m and F_m concur with Fig. 3. The signal strength varies from +0.27 dB to -0.28 dB, and the total variation is 1.75 dB.

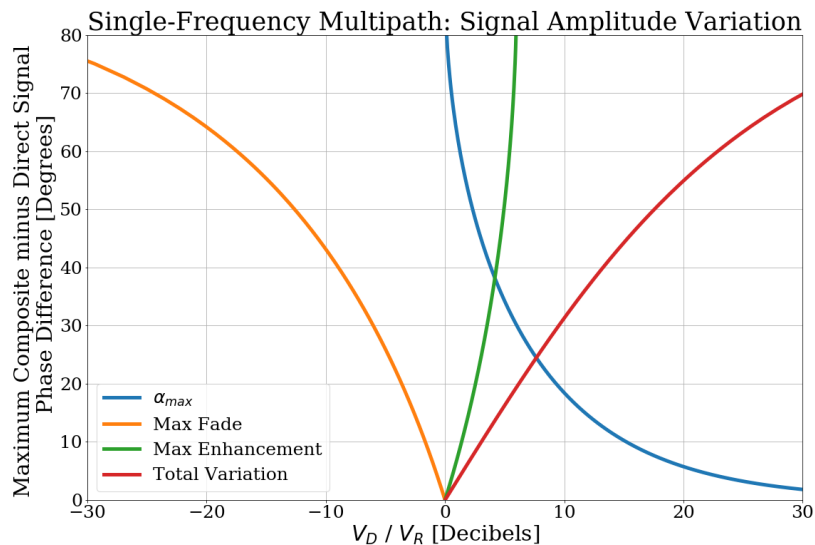


Fig. 3. Single Frequency Carrier Phase Error and Signal Amplitude Effects due to Multipath

4 Discriminator Function (Without Multipath Error)

A discriminator function is defined as the difference between early correlator and late correlator averages. The shape of the discriminator function is primarily influenced by the correlator spacing τ_d , written also as dT_C when normalized with the code chip width T_C . We shall later see how this correlator spacing mitigates the effect of the delayed reflected signal and curbs the multipath error.

The early (S_E) correlator and late (S_L) correlator samples in a discriminator function $D_c()$ are discussed in [2], Section 10.5, and are defined as

$$S_E(\Delta\tau) = \sqrt{C}R(\Delta\tau - \tau_d/2) \quad (6)$$

$$S_L(\Delta\tau) = \sqrt{C}R(\Delta\tau + \tau_d/2) \quad (7)$$

where C is the signal power, $\tau_d = T_C$ for wide correlators and $\tau_d < T_C$ for a narrow correlators and $R()$ is the autocorrelation function. The discriminator function $D_c()$ is defined as -

$$D_c(\Delta\tau) = S_E(\Delta\tau) - S_L(\Delta\tau) \quad (8)$$

It passes through the discriminator function passes through the origin where the delay estimation error $\Delta\tau$ is zero. These are shown in Fig. 4 for $\tau_d = T_C$, $0.5T_C$ and $0.1T_C$. As demonstrated in Fig. 4, in the absence of multipath, the function

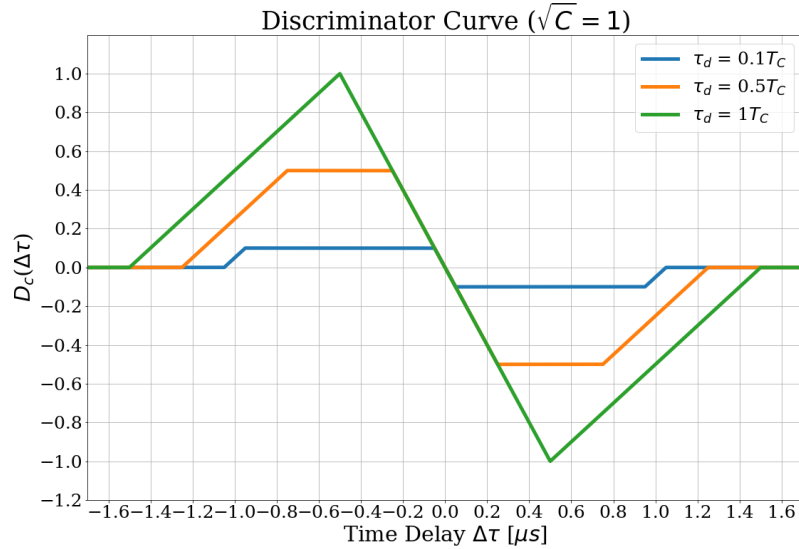


Fig. 4. Discriminator function curves for three different correlator spacing ($\tau_d = 0.1T_C, 0.5T_C, 1T_C$)

is zero at the origin, and its slope at the origin is independent of τ_d , though the apex of its triangle is truncated and its base shrinks progressively as τ_d lowers from $1T_C$ to $0.1T_C$. The results shown in Fig. 4 are of course not new. They are widely available in the literature, but they are shown here to lend confidence to the subsequent multipath errors for the NavIC frequencies.

5 Autocorrelation Function Perturbed by Multipath

When a direct signal is blended with a reflected signal, its triangle autocorrelation with the receiver-generated pure pseudo-random code is distorted, as explained in [2], Sec. 10.7. The reflected signal travels a greater distance and, hence, always arrives after the direct ray. However, it interacts constructively or destructively according to its relative phase with the direct signal, causing it to fade or enhance as illustrated earlier in Sec. III. The relative phase angle of the reflected signal from the direct signal varies from 0 to 360 degrees.

The reflected signal can cause the correlation peak to rise if it arrives in phase with the direct signal as demonstrated in Fig. 5 where the composite peak is slightly higher than the autocorrelation peak of the direct ray. Similarly, if the reflected signal arrives out of phase, the multipath signal interferes destructively with the direct ray and lowers the peak as demonstrated in Fig. 6. In Fig. 5-6,

$\Delta\tau_M$ is the multipath delay relative to the direct signal, and α is the multipath ratio V_R/V_D .

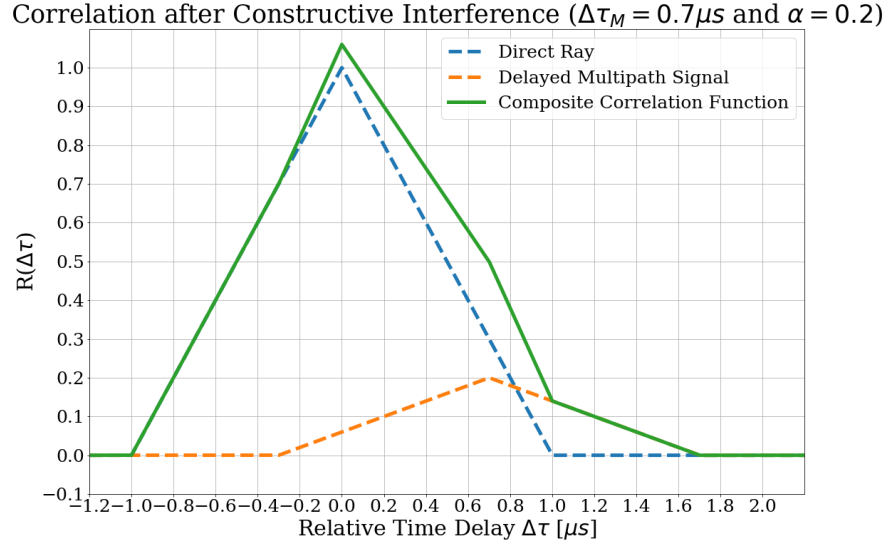


Fig. 5. Autocorrelation peak perturbed due to constructive interference

To calculate the delayed multipath autocorrelation function illustrated in Figs. 5-6, a function called $R_m()$ is defined that takes in a range of values for the delay estimation error $\Delta\tau$ (the same for direct ray and reflected ray), the time delay $\Delta\tau_M$ of the reflected signal relative to direct signal and multipath-to-signal amplitude ratio α . Using these parameters, and the autocorrelation function $R()$ defined by Eq. (1) previously, the autocorrelation function for reflected signal can be modelled as -

$$R_m(\Delta\tau) = \alpha R(\Delta\tau + \Delta\tau_M) \quad (9)$$

A threshold is defined for the multipath delay $\Delta\tau_M$ which distinguishes a short-delay multipath from a long-delay. Ref. [2] explains in Sec 10.7.1 that 'No errors exist when the rising edge of the delayed peak does not touch the late correlator sample'. Mathematically, the condition of long-delay multipath is expressed by the inequality

$$\Delta\tau_M \geq T_C + \frac{\tau_d}{2} \quad (10)$$

where recall that τ_d is the correlator spacing, equal to dT_C . A long delay multipath is demonstrated in Fig. 8 for $\Delta\tau_M = 1.6\mu s$ and $\tau_d = T_C$ or $d = 1$ and $T_C = 1\mu s$. In such cases, there is no effect of multipath on null tracking.

Correlation after Destructive Interference ($\Delta\tau_M = 0.7\mu s$ and $\alpha = 0.2$)

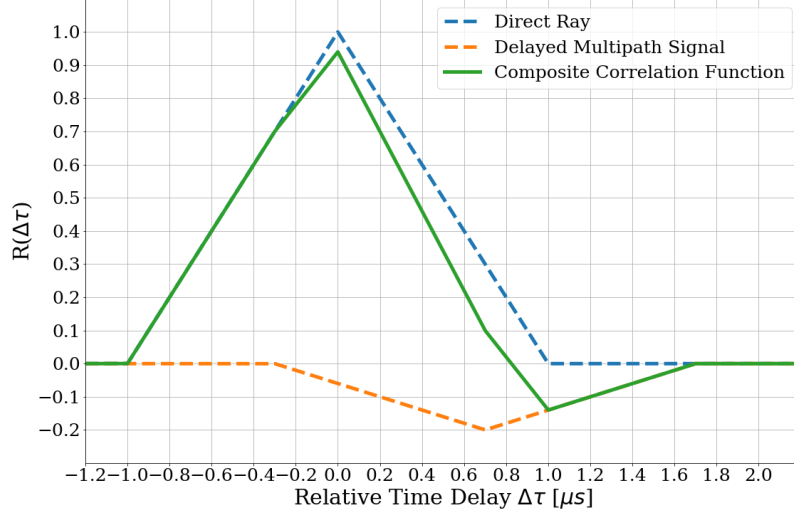


Fig. 6. Autocorrelation peak perturbed due to destructive interference

Correlation after Constructive Interference ($\Delta\tau_M = 1.6\mu s$ and $\alpha = 0.2$)

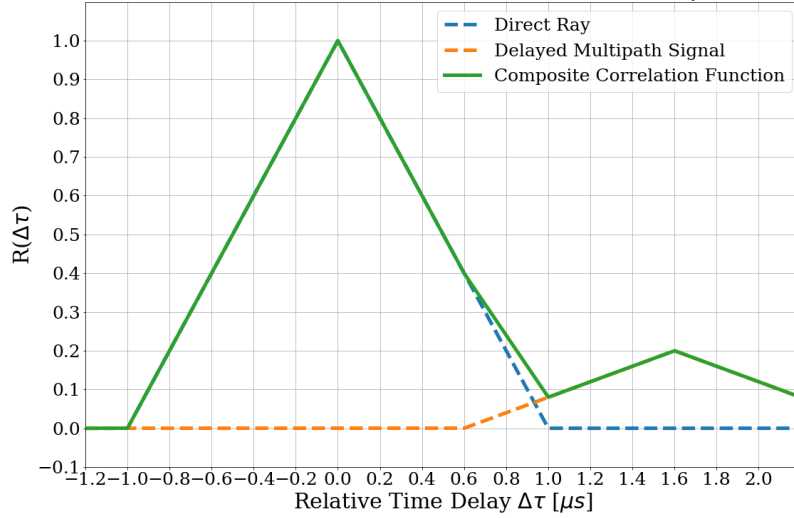


Fig. 7. Composite autocorrelation peak unchanged by a long-delay multipath (for wide correlator)

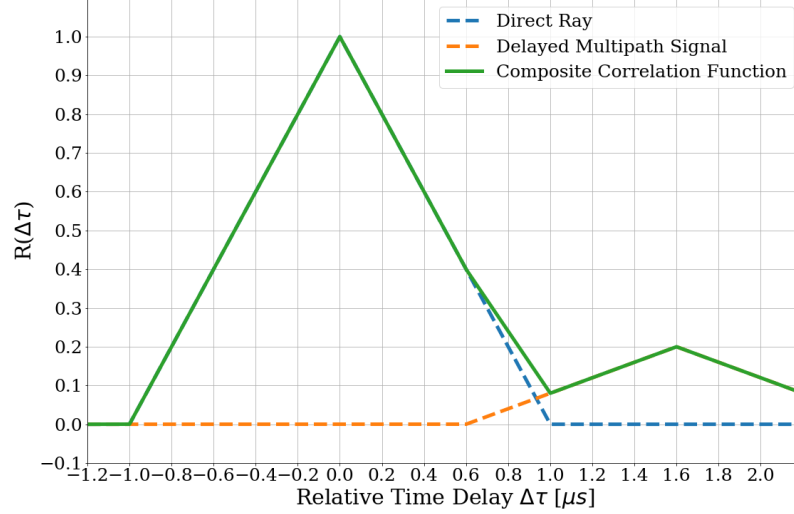
Correlation after Constructive Interference ($\Delta\tau_M = 1.6\mu\text{s}$ and $\alpha = 0.2$)

Fig. 8. Composite autocorrelation peak unchanged by a long-delay multipath (for wide correlator)

6 Multipath-Affected Discriminator Function

Since discriminator function is dependant on the autocorrelation function and - as we just observed - autocorrelation function gets perturbed by multipath, the discriminator function also gets affected by the presence of multipath. This is made clear by Fig. 9 which demonstrates how the discriminator function for same input parameters can differ when the multipath-to-signal ratio α becomes non-zero.

Brausch and Graass[4] developed a model of a discriminator function $D_c()$ affected by a single reflected signal. It is defined using the following two nonlinear equations -

Discriminator Function:

$$D_c(\tau) = [R(\tau + \tau_d) - R(\tau - \tau_d)] \cos \phi_m + \alpha[R(\tau + \tau_d - \Delta\tau_M) - (\tau - \tau_d - \Delta\tau_M)] \cos(\theta_m - \phi_m) = 0 \quad (11)$$

where the multipath-caused carrier phase tracking error (same as the one calculated by Eq. (2) using a different approach) is defined as

$$\phi_m(\tau) = \tan^{-1} \left(\frac{\alpha R(\tau - \Delta\tau_M) \sin \theta_m}{R(\tau) + \alpha R(\tau - \Delta\tau_M) \cos \theta_m} \right) \quad (12)$$

and relative phase of the multipath signal, θ_m , is related to the signal frequency and $\Delta\tau_M$ thus:

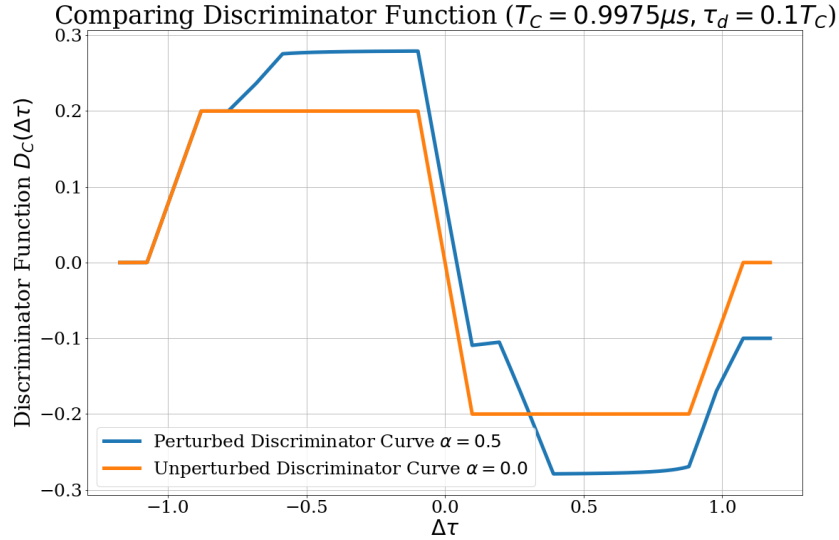


Fig. 9. Composite autocorrelation peak unchanged by a long-delay multipath (for wide correlator)

$$\theta_m = 2\pi\Delta\tau_M f \quad (13)$$

An algorithm was developed to solve (11) and (12) to determine the code delay estimation error τ (the same as $\Delta\tau$ used earlier) for a reflected signal time delay $\Delta\tau_M$ relative to the direct signal and the corresponding phase delay θ_m of the multipath relative to the direct signal. Henceforth, the solution to (11) and (12) i.e. the value of τ satisfying $D_c(\tau) = 0$ for ϕ_m defined by (12) would be referred to as τ^* .

Our objective is to solve the two non-linear functional equations (11) and (12) for τ and ϕ_m at a given multipath delay $\Delta\tau_M$ and the phase θ_m . We do this iteratively in an algorithm as explained below.

1. Assign $\Delta\tau_M$ the first value from a specified range $[\Delta\tau_M]$. $\Delta\tau_M$ is the additional traversal time of the reflected signal to arrive at the receiver antenna relative to the direct signal.
2. Compute the corresponding $\theta_m(\Delta\tau_M)$ with Eq. (13).
3. Assign τ the first value from a specified range $[\tau]$ (in our case $[\tau] = [-0.1T_C, 0.1T_C]$).
4. Using τ and $\theta_m(\Delta\tau_M)$, compute $\phi_m(\tau)$.
5. Plug in the calculated value of $\phi_m(\tau)$ in the expression for $D_c(\tau)$ and evaluate the complete expression.
6. Check if $D_c(\tau) = 0$ (or its approximation to the desired limit of zero).
7. If **YES** then:

- (a) Store the value of τ (call this τ^*) and $\phi_m(\tau^*)$ for the corresponding $\Delta\tau_M$ in the memory.
 - (b) Assign $\Delta\tau_M$ the next value in the range $[\Delta\tau_M]$.
 - (c) Move to Step 2 and repeat for all values in $[\Delta\tau_M]$.
 - (d) Thus repeat for all values in $[\Delta\tau_M]$
8. If **NO** then:
- (a) Assign τ the next value from the range $[\tau]$.
 - (b) Move to Step 4 and repeat.

By the time the algorithm has iterated through all values of $\Delta\tau_M$, it should have a range of corresponding code tracking error τ^* and carrier tracking error $\phi_m(\tau^*)$ stored in the memory.

7 Single-Reflection Errors of GPS and NavIC Signals: Illustrations

7.1 GPS Signal L1 Results for Validation

The above algorithm generated Fig. 10 for the GPS L1 frequency $f = 1575.42MHz$ with a narrow correlator spacing $\tau_d = 0.1T_C$, and the multipath ratio $\alpha = 0.6$. The upper and lower bounds in red in Fig. 10 correspond to maximum and minimum code tracking error. This envelope is discussed in greater detail in Sec. VII. In Fig. 10 we observe that the negative peaks of the code error are even greater in magnitude than the multipath delays that cause them. Also, as is well known, the errors are non-sinusoidal with a growing negative bias. These results agree with those in [4].

To compare our results with *Brodin* [5], the code tracking error τ^* nanoseconds needed to be converted to degrees. This is done as follows. A code chip pulse width is $T_C = 0.9775\mu s$ and it is equivalent to one wavelength i.e. 360° . Hence, the wavelength of each chip is

$$\lambda_{code} = c \times T_C = 299.79246m/\mu s \times 0.9775\mu s = 293.05m$$

Therefore, the code wave is $360^\circ/293.05m = 1.23$ degrees per meter. Further, the initial multipath delay $\Delta\tau_M$ relative to the direct signal was $300ns$ i.e. 89.91 meters or ~ 90 meters. Over a multipath phase change of 360° , the multipath delay changes by c/f where f is frequency of the signal. In the case of GPS L1 signal, a phase change of 360° corresponds to 0.19 meters. Since, $0.19m \ll 89.91m$, the multipath delay is assumed to be constant and the relative phase is varied independently in Fig. 11. The range for code tracking error ($\pm 12^\circ$) in our calculations differ from the calculations presented in *Brodin* [5] ($\pm 9^\circ$). This is likely due to a mismatch in one of the constant parameters that is used in the calculation.

The results in Fig. 11, unlike those in Fig.10, are symmetric about the x-axis because these are for $\tau_d = 0.1T_C$, $\alpha = 0.5$, and the initial multipath delay

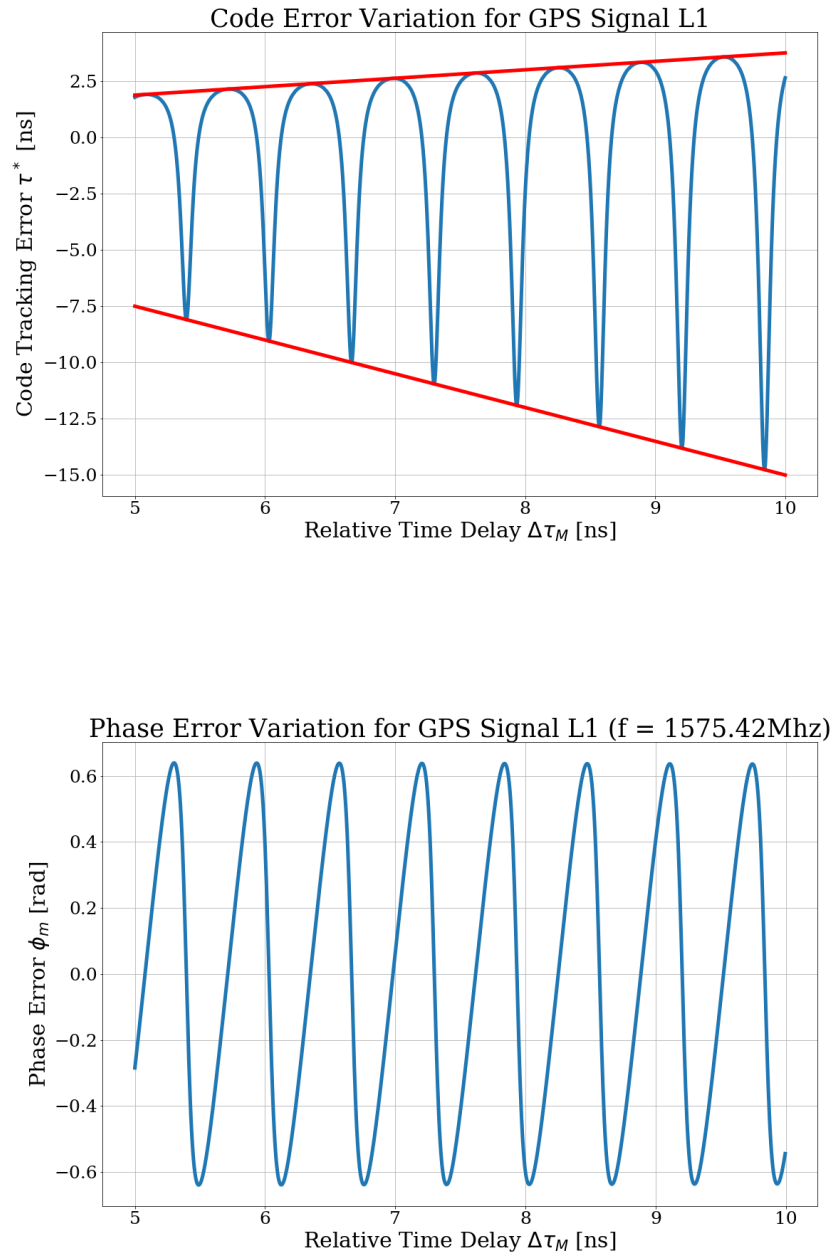


Fig. 10. Code error and phase error oscillations in GPS Signal L1 versus reflected wave time delay for the multipath amplitude ratio of 0.6

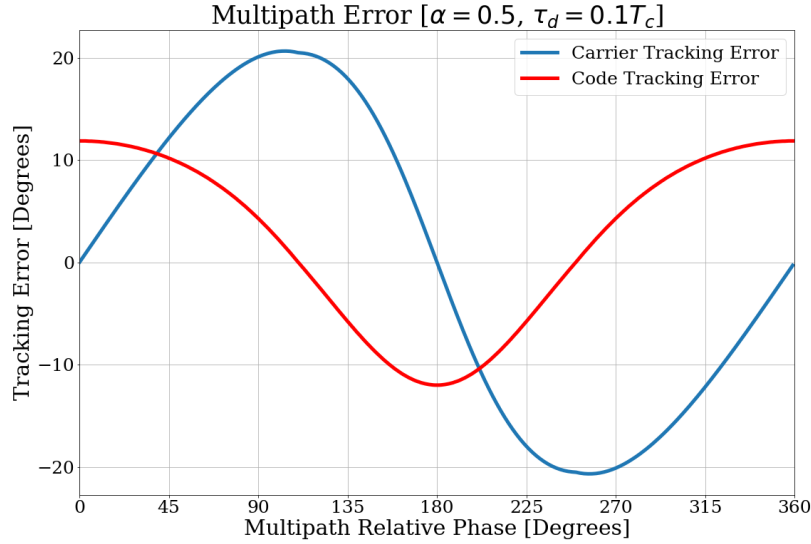


Fig. 11. Code and Carrier Error variation across one period of multipath relative phase (initial $\Delta\tau_M = 300$ ns)

$\Delta\tau_M = 300$ ns. The code delay estimation error plateaus at the multipath delay [4] (as explained further in Sec. VII)

$$\Delta\tau_{M\text{plateau}} = (1 + \alpha)\tau_d$$

For the parameters just stated, $\Delta\tau_{M\text{plateau}} = 75$ ns, whereas the results in Fig. 11 are for $\Delta\tau_M = 300$ ns. For these parameters, the code delay estimation error oscillates between its equal positive and negative limits, though the error is positive for a longer part of the period than they are negative.

7.2 Multipath Errors for NavIC Signal

The above algorithm was applied to NavIC signals, and the results are shown in Figs. 12-14. The central frequency of NavIC L5 band is $f_{L5} = 1176.45\text{MHz}$ and for S-band is $f_S = 2492.02\text{MHz}$. The corresponding wavelengths are 0.255 m and 0.120 m, respectively. Because the wavelength of NavIC L5 (0.255 m) is longer than that of the GPS L1 (0.19 m), the multipath oscillations periods are longer and the oscillations are slower in Fig. 12 than those for GPS in Fig. 10. On the other hand, since the S-band wavelength 0.12 m is nearly half of the L5 wavelength, the multipath oscillations for the S-band in Fig. 14 are twice as many as that for the L5 signals in Fig. 12. We also see that the negative peaks of the code errors are greater in magnitude than the positive peaks, as is typical

with the multipath errors, and the envelopes cradle the errors as expected. The code delay estimation errors in nanoseconds in the above figures is converted to meters easily by recalling that 1 ns = 0.3 m.

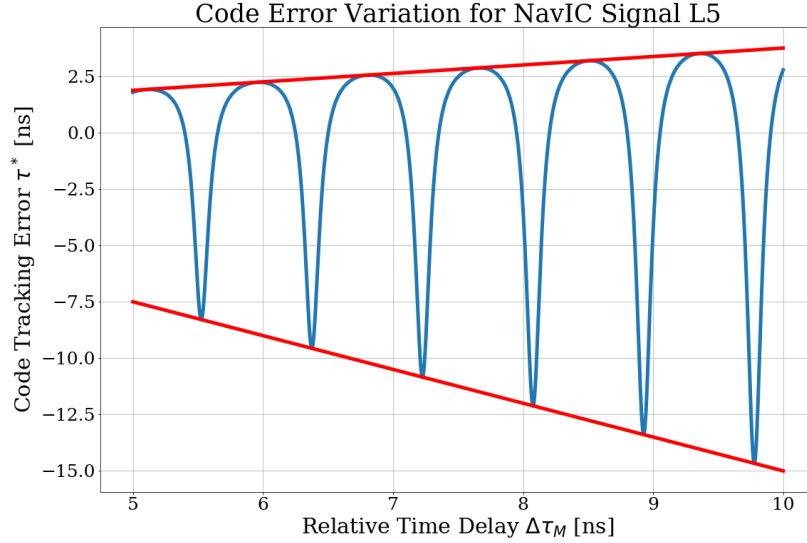


Fig. 12. Code Error Oscillations for NavIC L5 Frequency

8 Multipath Error Envelopes

As mentioned earlier, the multipath error oscillates between a positive limit and negative limit as the phase of the reflected signal varies relative to the direct signal with the continuous change in the satellite elevation angle.. *van Nee* presented these upper and lower bounds – the multipath error envelopes – in [12], and they are illustrated here to gain familiarity with them and then to draw them for the NavIC multipath errors in Figs. 12-14. The upper bound of the envelope is caused by the constructive interference and the lower bound by the destructive interference. These two bounds constitute the multipath error envelopes.

To calculate the upper bound of the code multipath error, τ_{max}^* , two constants are defined [12]:

$$a = \tau_d \left(\frac{1 + \alpha}{2} \right)$$

$$b = T_C - \tau_d \left(\frac{1 - \alpha}{2} \right)$$

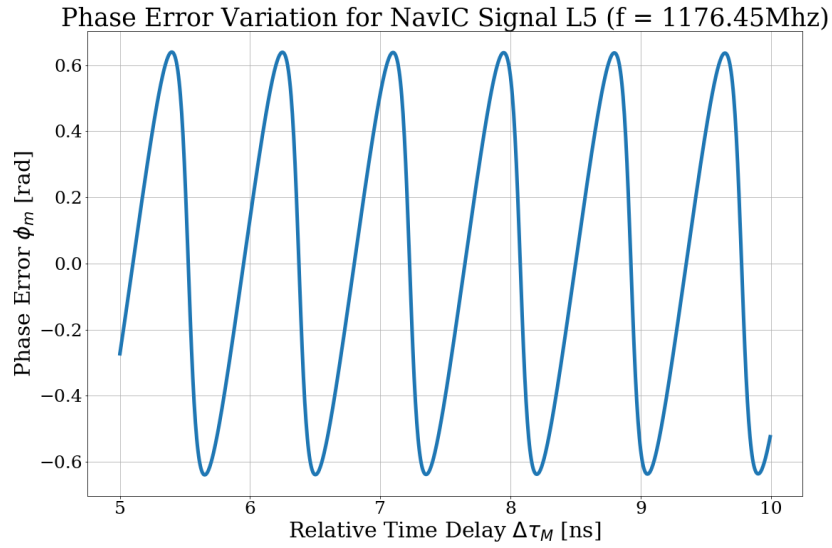


Fig. 13. Phase Error Oscillations for NavIC L5 Frequency

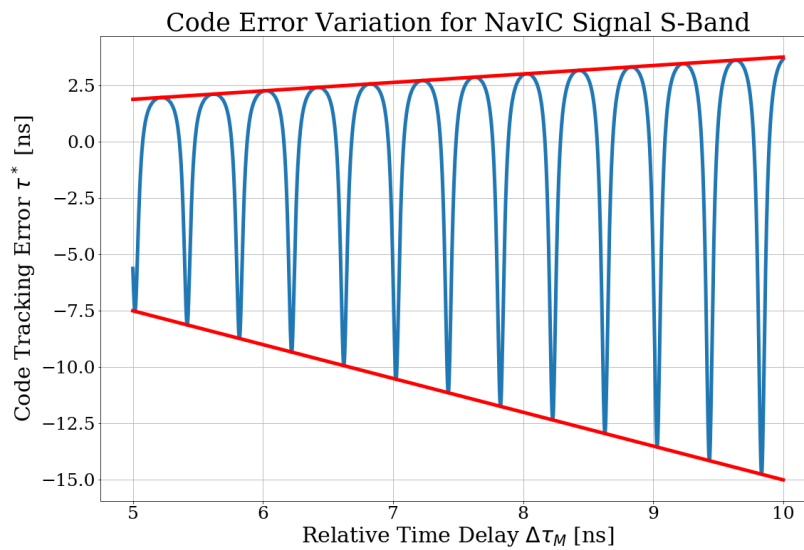


Fig. 14. Code Error Oscillations for NavIC S-Band Frequency

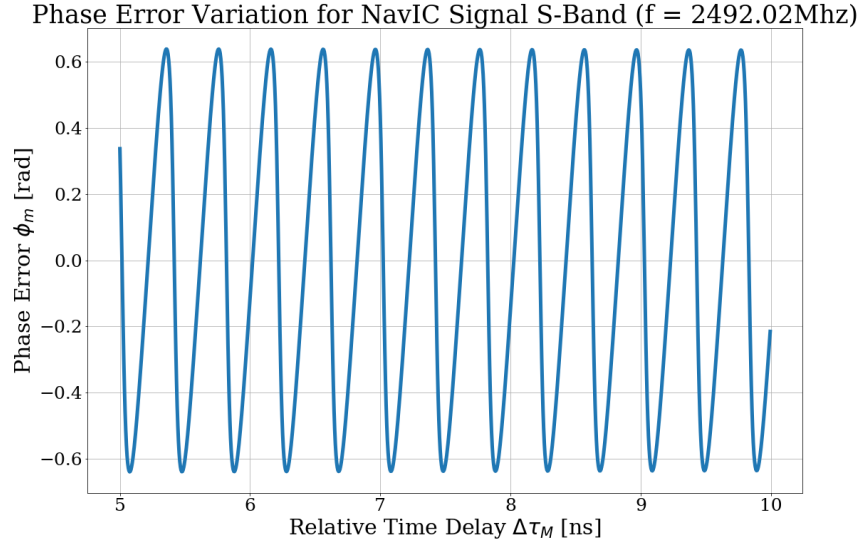


Fig. 15. Phase Error Oscillations for NavIC S-Band Frequency

These constants parametrize the piece-wise function for the multipath error envelope -

$$\tau_{max}^* = \begin{cases} \frac{\alpha\Delta\tau_M}{1+\alpha} & \text{if } 0 \leq \Delta\tau_M < a \\ \frac{\alpha\tau_d}{2} & \text{if } a \leq \Delta\tau_M \leq b \\ \frac{\alpha}{2-\alpha}(T_c + \tau_d/2 - \Delta\tau_M) & \text{if } b < \Delta\tau_M \leq T_c + \tau_d/2 \\ 0 & \text{if } \Delta\tau_M > T_c + \tau_d/2 \end{cases} \quad (14)$$

To calculate the lower bound τ_{min}^* caused by the destructive interference, all instances of α in (14) are replaced by $-\alpha$. Plotting the two bounds together gives us Fig. 16 where the code delay estimation error is presented in both microseconds and distance (1ns \approx 0.3m). These results are indeed the same as in Fig. 10.23 [2], where the multipath amplitude is 12 dB ($10^{-12/20} = 0.25 = \alpha$) below the amplitude of the direct ray. The effect of τ_d in Fig. 16 is discussed next.

8.1 Effect of Correlator Spacing

Fig. 16 shows that a narrower correlator spacing ($1 T_C$ to $0.5 T_C$ to $0.1 T_C$) de-escalates the code delay estimation error envelope. The error envelope is not symmetric about the x-axis as we saw earlier in Figs. 10, 12 and 14 and now in Fig. 16. Even though the positive and negative limits are numerically equal,

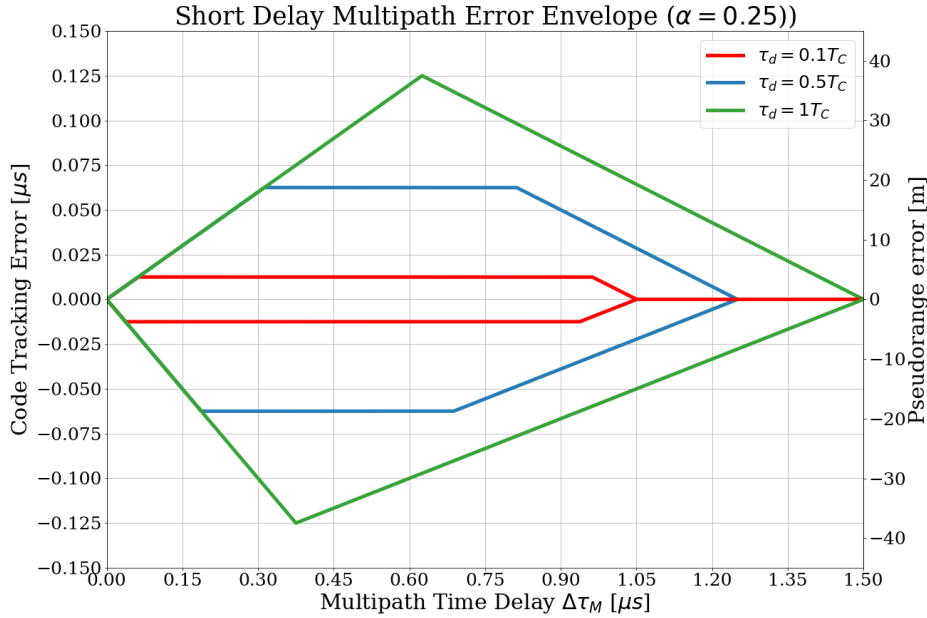


Fig. 16. Multipath Error Envelopes for three different correlator spacing ($\tau_d = 0.1T_C, 0.5T_C, 1T_C$)

the negative error reaches its limit faster than the positive error, thus causing asymmetric oscillatory errors with a time varying bias. Ref. [12] shows that for $\tau_d < T_C$, when the multipath delay exceeds $(1+\alpha)\tau_d/2$, the code delay estimation error reaches its limits on both sides positive and negative. Additional features of the envelope seen in Fig. 16 are well known, so they are not discussed further.

8.2 Effect of Multipath-to-Signal Amplitude Ratio

Surfaces with poor reflective qualities attenuate the incident signals, and result in a low value of multipath-to-direct amplitude ratio α . This ratio depends also on the multipath rejection properties of the receiver antenna. The effect of multipath-to-direct amplitude ratio on the code delay estimation error is portrayed in Fig. 17 for $\tau_d = T_C$. The lower is the reflection coefficient, α , the lesser is the multipath-caused code delay error, as we see the shrinking envelopes in Fig. 17 with the reduction in α . In case of no reflections, $\alpha = 0$.

8.3 Mean Error

As evident from the envelopes in Figs. 16-17 and also from Figs. 11-14, even though the positive and negative plateaus of the envelope are quantitatively equal, the signals take different durations of multipath delays to reach those plateaus. Hence the error envelopes are asymmetric about the x-axis. This means

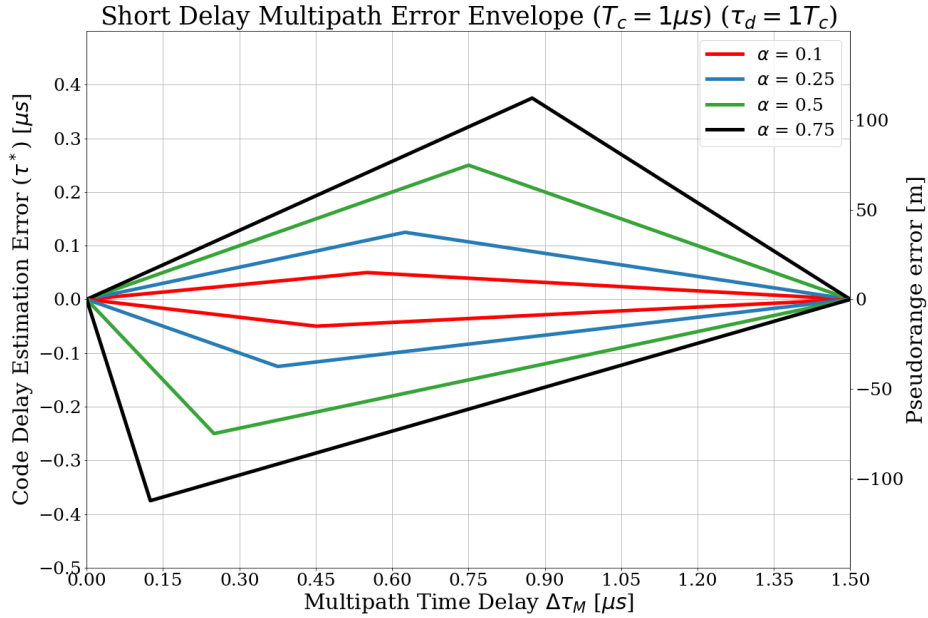


Fig. 17. Multipath Error Envelopes for different multipath-to-direct amplitude ratio ($\alpha = 0.1, 0.25, 0.5, 0.75$)

that the multipath-caused mean error vs. $\Delta\tau_M$ is nonzero. *Breiviek et. al* [7] discuss this non-zero bias error for a correlator-spacing $\tau_d = T_C$. For a given path difference $\Delta l = c\Delta\tau_M$ between a direct signal and its reflected signal, the bias ϵ_M (in meters) is

$$\epsilon_M = -c\Delta\tau_M \left(\frac{\alpha^2}{1 - \alpha^2} \right) \quad (15)$$

for

$$\Delta\tau_M \leq \frac{1 - \alpha}{2} \tau_d$$

Fig. 18 depicts a magnified initial region of the short-delay multipath error in Fig. 17 and the code delay estimation error bias for the multipath ratios = 0.1 and 0.25. The results show that the bias increases with α and the additional distance a reflected signal traverses.

9 NavIC Multipath Errors of a Stationary Receiver - A Case Study

In the preceding sections, we have explored the relationship between the extra time $\Delta\tau_M$ the reflected signal takes to reach the antenna relative to the direct signal, and the code phase and carrier phase errors, but we have not shown what determines $\Delta\tau_M$. Indeed, if $\Delta\tau_M$ is fixed, then the code and carrier phase

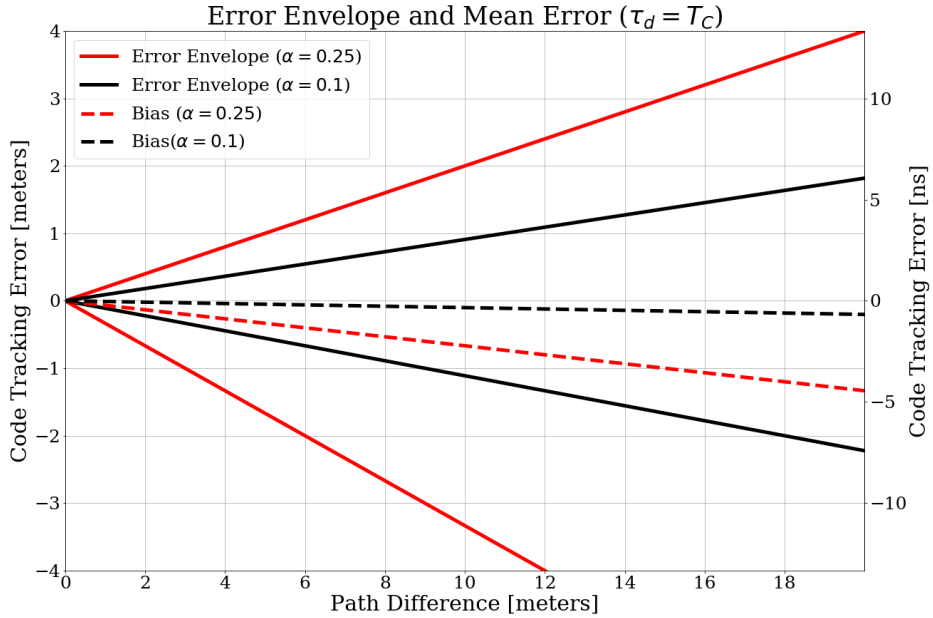


Fig. 18. Multipath Error Envelopes and the associated bias for different Multipath-to-Signal amplitude ratios ($\alpha = 0.2, 0.5$)

errors will be constant. So we will now investigate the dependence of $\Delta\tau_M$ on the physical time t and the types of the reflectors.

Hofman-Wellenhof et al. [10] show that the extra path length of a signal from a satellite at an elevation angle el , reflected from the ground and reaching the receiver antenna at a height h in the extra time $\Delta\tau_M$ relative to the direct signal is

$$\Delta l(t) = c\Delta\tau_M = 2h \sin el(t) \quad (16)$$

For a vertical reflector at a normal distance h from the antenna, with the normal at an azimuth angle az relative to the satellite signal, the reflected signal travels the extra length [3]

$$\Delta l(t) = 2h \cos el \cos az \quad (17)$$

In both cases the corresponding phase angle θ_m of the reflected signal relative to the direct signal, used in the preceding sections, at the antenna will be

$$\theta_m = 2\pi f \Delta\tau_M - \phi_R = 2\pi f (\Delta l/c) - \phi_R \quad (18)$$

where ϕ_R is the change in the phase angle (180 degrees) due to the reflection. The above variables ($\Delta\tau_M$, Δl and θ_m) vary with time as elevation and azimuth angles of the satellite signals change. These variations in the case of the 24-hour NavIC satellites for an Accord receiver [11] are illustrated in a sky plot Fig. 19 at IIT Gandhinagar and in Fig. 20 as a function of time over 24 hrs from 5:00

AM to the next day 5:00 AM at IIT Indore. The azimuth and elevation angles vary greatly but slowly for the geosynchronous satellites in the inclined orbits (GSO) and much less for the essentially equatorial geostationary orbits (GEO). Also, for the GSO satellites the range of variation of azimuth is greater than that of the elevation angles. The significance of this will become apparent below.

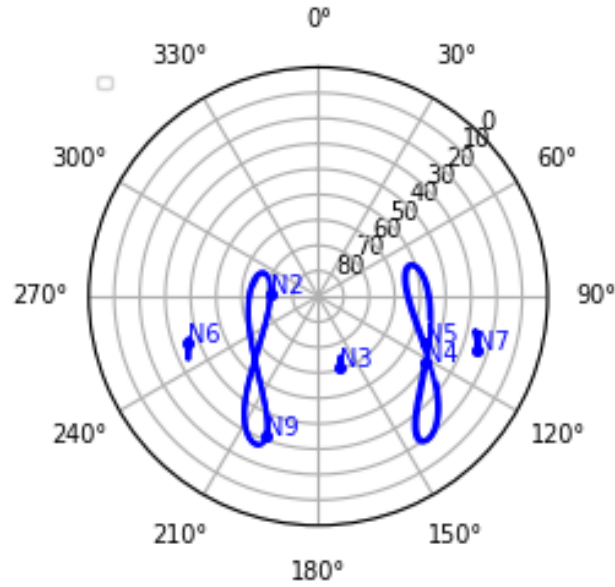


Fig. 19. Variations in the case of the 24-hour NavIC satellites for Accord receiver at IIT Gandhinagar as a sky plot

9.1 Frequency Bandwidth of the Reflected Signals

As the elevation and azimuth angles of the satellite signals change, the extra length of a single reflected signal changes. For a horizontal reflector, the rate of change is

$$\dot{\Delta}l = 2h \cos(el) \dot{el} \quad (19)$$

and for a vertical reflector the rate is

$$\dot{\Delta}l = -2h[\cos(el) \sin(az) \dot{az} + \cos(az) \sin(el) \dot{el}] \quad (20)$$

and the corresponding rate of change of the relative multipath phase angle is

$$\dot{\theta}_m = 2\pi f_M = 2\pi \frac{\dot{\Delta}l}{\lambda} \quad (21)$$

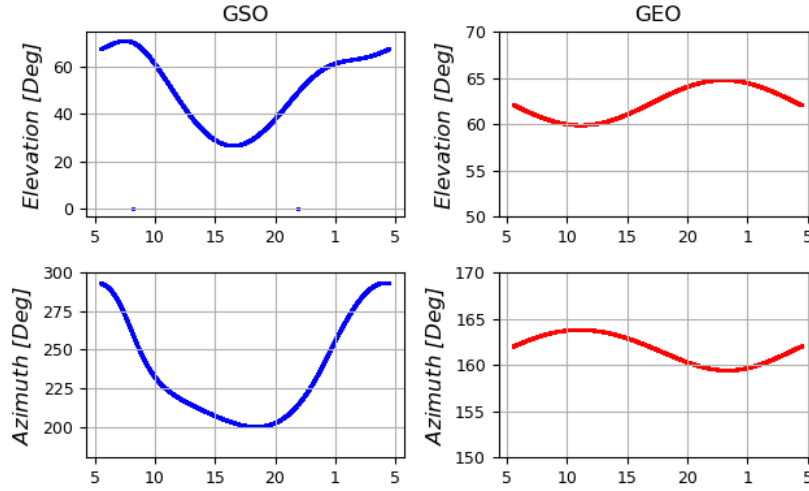


Fig. 20. Variations in the case of the 24-hour NavIC satellites for Accord receivers at IIT Indore as a function of time

as shown in [16] for horizontal reflectors.

van Nee [6][12] calls f_M the fading bandwidth and called to attention the receiver position uncertainty caused by the multipath error and therefore its potential influence on the search of the correct frequency bin in the delay lock loop for signal acquisition.

9.2 Accord Receiver Doppler Shift Accuracy Specification

As *van Nee* [6][12] noted, *Smith and Graves* [13] determined that for the 12-hour GPS satellites a 1m receiver position error could cause a 1 mHz Doppler frequency error if the earth's rotation rate is ignored and 1.38 mHz if it is not. For the 24-hour NavIC satellites, *Althaf et al.* [14] showed that for an antenna of 2m height a ground reflection of a NavIC GSO satellite signal causes a Doppler shift of 0 to + / - 1.6 mHz, so the shortest period of the Doppler shift is 625 s, or ~10 minutes. The equations of f_M shown above reveal that a vertical reflector will cause greater Doppler shift than a horizontal reflector because both azimuth and elevation angles vary for a vertical reflector whereas only elevation angle varies for a horizontal reflector. The related numerical results for a vertical reflector are not available, but the f_M of the NavIC signals may rise up to no more than 10 mHz (0.01 Hz) and the shortest period would be ~ 100 s.

The Accord receiver antenna's multipath rejection ratio, though not known, is discussed in [9] and is expected to be between 10 dB (3.2) to 34 dB (50.1). Also, the Accord receiver's velocity accuracy is specified to be 0.2 m/s (1σ), which is equal to 0.8 Hz (1σ) for L5 signal (wavelength 0.255 m) and 1.67 Hz (1σ) for the S signal (wavelength 0.12 m). Assuming that an average PDOP

(position dilution of precision) of the NavIC signals is 4, the expected frequency error jitter in the range rate observables for L5 would be $0.8 \text{ Hz} / \text{PDOP} = 0.2 \text{ Hz}$ (1σ) and similarly for the S signal, 0.4 Hz (1σ). So, we anticipate that the RSS of the frequency jitter caused by thermal noise and multipath error will be less than these specifications. A related illustration is shown below.

9.3 Real Multipath Errors in NavIC Signals: Illustration

An example of the receiver multipath error and the corresponding profiles of the elevation angles versus local time from 9:30 PM to 5:30 AM for 8 hours are shown in Fig. 21 for six NavIC satellites for L5 frequency in the left column and S frequency in the right column. These errors are real, obtained from the dual-frequency code phase and carrier phase observables using the well-known formula with twice the iono delay term removed [14] but the ambiguity and noise not removed. Also, the receiver antenna is in the Workshop Building with several potential reflectors in the surroundings, and therefore the reflected signals may have a general Rayleigh distribution.

As commented above, the multipath error frequencies vary in Fig. 21 during the eight hours shown since the six signal elevation angles and azimuth angles vary as typified in Figs. 19-20 for a GEO satellite and a GSO satellite. Because the satellites are spread out in the constellation, the six elevation and azimuth angle profiles and their rates are varied and the slow frequencies and the fast frequencies are randomly scattered in time. Since the S wavelength (0.12 m) is nearly half of the L5 wavelength (0.255 m), the S-multipath frequencies are twice the L5 multipath frequencies, as we observe in the left and right columns of Fig. 21.

The left column results in Fig. 21 is for the L5 frequency and the right column is for the S frequency. In the left top plot, the low-frequency (not the noise) oscillations are the slowest, with a period of ~ 40 minutes, and the trough-to-peak ~ 4 m when the elevation angle is near its minimum value, ~ 27 deg, and its rate of change is slow – zero or nearly zero, because then the multipath oscillation frequency f_M is ~ 0 . As the elevation angle increases to ~ 60 deg, the oscillations speed up and amplitudes lower down.

In the left top-fourth plot in Fig. 21, when the elevation angle approaches its peak, 55 deg and its slope nears zero, the oscillations slow down, with a period of ~ 1 hr and trough-to-peak ~ 2 m. In the left top-fifth plot for a GEO satellite, the elevation angle changes little, so the elevation rate is nearly zero, and therefore the multipath error is highly noisy with smaller amplitudes and slow oscillations, ~ 1 m, with a drifting bias as expected.

As stated above, the S1 frequency multipath errors in the right column are twice as fast as the L5 multipath error in the left column. The trough-to-peak amplitudes in both frequencies are about the same for all satellites except for the last one in the left-bottom plot where the trough-to-peak amplitude is ~ 6 m.

Fig. 21 is not over a 12-hour period, so complete ranges of the elevation angles of the satellites are not covered, and therefore we do not have a full spectrum of

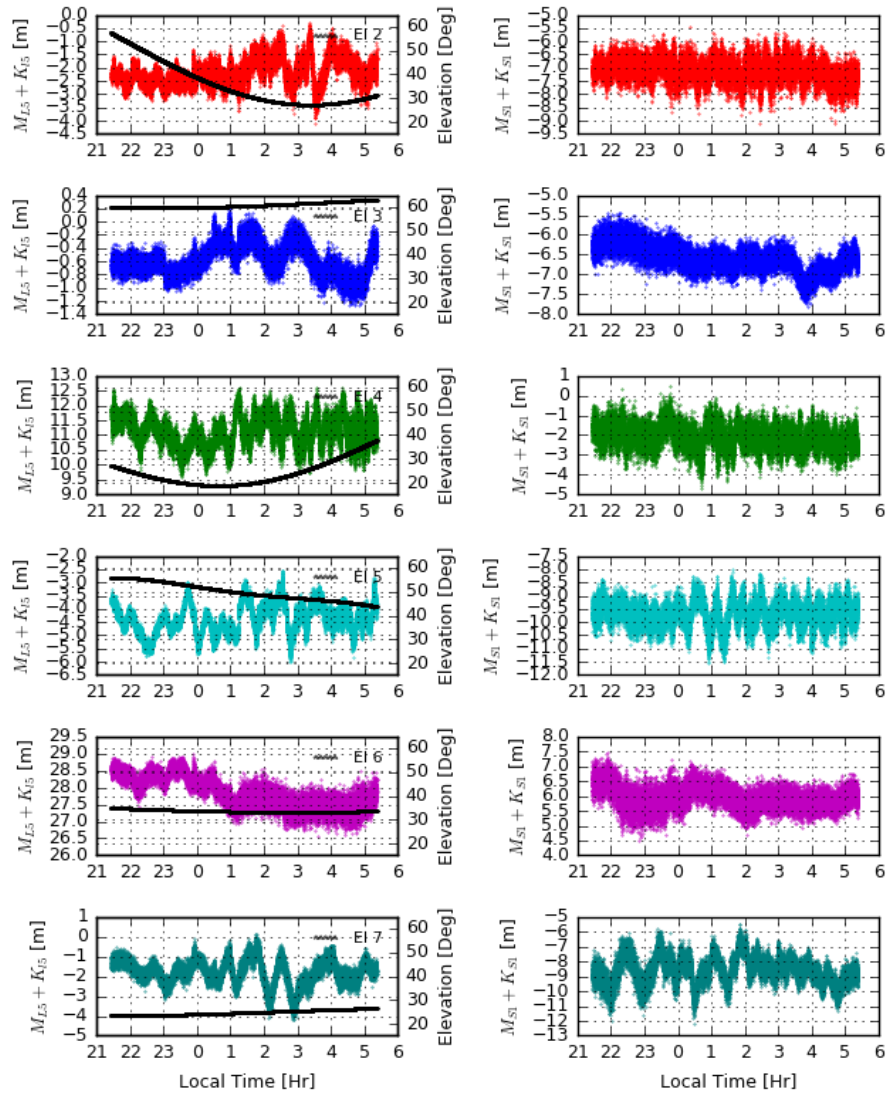


Fig. 21. Multipath in L5 and S1 Frequencies and Elevation vs. Time in Workshop Building – March 12, 2021

the multipath errors in these plots. Also, as shown in the analysis, the multipath error depends also on the relative azimuth angle of the reflector and its rate, but the azimuth angles are not shown here, so our comments here are not complete.

The multipath errors are mixed with the receiver noise and fixed ambiguities, and they need to be separated using the receiver delay lock loop, phase lock loop

and frequency lock loop parameters and performance characteristics, as Braasch has demonstrated in [15].

The accuracy of the Accord receiver position estimate is stated to be 10 m (1σ) without SBAS [Space-Based Augmentation System] and 6 m (1σ) with SBAS [12]. A SBAS provides corrections for the navigation satellites position errors, satellite clock errors and ionospheric delays. The NavIC signals provide these corrections, similar to the GAGAN system for civil aviation services. With typical multipath error illustrated in Fig. 21, the receiver's position estimation accuracies are shown in [9] and the Accord receiver meets its specifications well.

10 Conclusion

The paper presents an overview of the code phase and carrier phase errors caused by a single reflected path, and illustrates them for the first time for NavIC signals in both frequencies L5 and S1. Real multipath errors are also illustrated for a NavIC receiver site at IIT Indore campus for both signal frequencies L5 and S1, and the causes of their substantial differences are identified. If no special efforts are made in the receiver or its antenna design and in the antenna's installation at any ground location, short-delay multipath errors of several meters are inevitable. Since these errors are non-sinusoidal, oscillatory with nonzero mean and long periods, they hinder accurate estimation of carrier phase ambiguities and thus high-accuracy positioning. Further, unlike other errors, multipath errors compound with between-receiver differencing and between-satellite differencing, so they preclude high-accuracy relative navigation for a stationary baseline as well. For this reason, several investigators have attempted in the past to estimate the multipath errors using their relationship with the C/N0 of the signal and compensate for them. However, Bilich et al. [16] have expressed their concerns over the extraordinary effort required for this estimation and yet relatively small returns in their mitigation. For this reason, it seems more cost-effective to use instead high-accuracy receivers with choke ring antennas for essentially a complete removal of the multipath error.

Acknowledgment

We are grateful to Space Application Centre, Indian Space Research Organisation for supporting this study as part of the NGP-17 project.

References

1. Blewitt G. "Basics of GPS Technique: Observation equations". In Geodetic Applications of GPS. 1997.
2. Misra P. and Enge P. "Global Positioning System: Signals, Measurements and Performance". 1997.
3. Doherty P. H., Bishop G. J. and Klobuchar J. A. Multipath effects on the determination of absolute ionospheric time delay from GPS. Radio Science.
4. Braasch M. S. and van Graas F. Mitigation of Multipath in DGPS Ground Reference Stations. 1992.
5. Brodin G. GNSS Code and Carrier Tracking in the Presence of Multipath. 1996.
6. van Nee R. D. J. GPS Multipath and Satellite Interference. 1992.
7. Breivik K., Enge P., Forssell B., Kee C. and Walter T. Detection and Estimation of Multipath Error in GPS Pseudorange Measurements Using Signal-to-Noise Ratio in a Stationary Single-frequency Receiver. 1996.
8. Parkinson, B. W. and Spilker Jr., J. J., (Eds.), Global Positioning System: Theory and Applications, Vol. 1, Chapter 14. Multipath Effects, pp. 547-568.
9. Althaf, A., and Hablani, H., "NavIC Signals Multipath Analysis, Estimation and Mitigation for High-Accuracy Positioning," ION ITM GNSS 2020, pp. 2878-2895
10. Hofmann-Wellenhof, B., Lichtenegger, H., and Wasle, E., GNSS – Global Navigation Satellite Systems, Springer 2008
11. IRNSS-GPS-GLONASS-GAGAN Receiver Brochure, Accord Software Systems Private Ltd., Rev. 1.1 Jan. 2016
12. van Nee, R. D. J., Multipath Effects on GPS Code Phase Measurements, ION GPS 1991, pp. 915-924
13. 5. Smith, C. A., and Graves, K. W., Sensitivity of GPS Acquisition to Initial Data Uncertainties, Navigation: Journal of the ION, Vol. 31, Fall 1984, pp. 220-232
14. Althaf, A., and Hablani, H., Assessment of errors in NavIC observables for stationary receivers, Navigation: Journal of ION, 2020, pp. 347-364
15. Braasch, M. S., "Isolation of GPS Multipath and Receiver Tracking Errors, ION NTM 1994, pp. 511-521
16. Bilich, A., Larson, K. M., and Axelrad, P., "Modeling GPS phase multipath with SNR: Case study from the Salar de Uyuni, Boliva," Journal of Geophysical Research, Vol. 113, 2008, B04401